Received: 3 November 2020 | Revised: 22 December 2020 | Accepted: 13 January 2021

DOI: 10.1002/asl.1027

RESEARCH ARTICLE

Atmospheric Science Letters RMetS

Interdecadal variability of intensity of the Madden–Julian oscillation

Ziyue Wang[1] | **Tim Li**[1,2] | **Ying Sun**[3]

[1]Key Laboratory of Meteorological Disaster, Ministry of Education (KLME)/ Joint International Research Laboratory of Climate and Environmental Change (ILCEC)/Collaborative Innovation Center on Forecast and Evaluation of Meteorological Disasters (CIC-FEMD), Nanjing University of Information Science and Technology, Nanjing, China

[2]International Pacific Research Center, Department of Atmospheric Sciences, School of Ocean and Earth Science and Technology, University of Hawaii at Manoa, Honolulu, Hawaii

[3]National Climate Center, Laboratory for Climate Studies, China Meteorological Administration, Beijing, China

Correspondence
Tim Li, Department of Atmospheric Sciences, University of Hawaii at Manoa, Honolulu, HI 96822, USA.
Email: timli@hawaii.edu

Funding information
National Natural Science Foundation of China, Grant/Award Number: 42088101; National Key R&D Program of China, Grant/Award Number: 2018YFA0605604; National Oceanic and Atmospheric Administration, Grant/Award Number: NA18OAR4310298; National Science Foundation, Grant/Award Number: AGS-20-06553

Abstract

The interdecadal variability of intensity of the Madden–Julian oscillation (MJO) during boreal winter was investigated based on two reanalysis datasets (NOAA 20CR and ERA-20C). Both the reanalysis datasets reveal statistically significant power spectrum peaks at 12–20-year periods. A composite analysis shows that during the active interdecadal phase, eastward propagating MJO activity was strengthened over the equatorial warm pool expanded from the Indian Ocean (IO) to the western Pacific (WP). The cause of the enhanced MJO variability was attributed to the interdecadal change of background mean precipitation in situ. A further diagnosis shows that the increase of the background precipitation over the Maritime Continent and the WP was attributed to interdecadal warm sea surface temperature (SST) anomalies in situ, whereas the increase of the precipitation over the IO resulted from the local convective instability due to the increase of wind induced surface evaporation and moisture. The strengthened background precipitation impacted the MJO strength through the increase of the interdecadal background moisture in the lower and middle troposphere induced by anomalous vertical moisture advection.

KEYWORDS

interdecadal variability, Madden–Julian oscillation, modulation of MJO strength by interdecadal background mean state

1 | INTRODUCTION

The Madden–Julian oscillation (MJO) is the most prominent intraseasonal mode in the Tropics. It was first discovered by Madden and Julian (1971; 1972). The MJO is characterized by eastward propagating large-scale convective anomalies with maximum amplitude being confined near the equator (Lau and Chan, 1986). It has a horizontal pattern of a Kelvin–Rossby wave couplet (Wang and Rui, 1990; Li and Wang, 1994; Salby *et al.*, 1994; Wang and Li, 1994) and a westward tilting vertical structure (Sperber, 2003; Wang *et al.*, 2017). The MJO

exhibits wide spectrum peaks with a typical period at 20–100 days (Li and Hsu, 2017) and a planetary zonal scale. The former is closely linked to slow eastward phase propagation (Lau and Peng, 1987; Wang and Li, 1994; Li and Hu, 2019), whereas the latter is possibly attributed to a nonlinear positive-only heating (Li and Zhou, 2009) or a cloud-radiative feedback (Adames *et al*., 2017). The MJO is often initiated from the tropical western Indian Ocean (IO) (Zhao *et al*., 2013) and dissipated over the cool waters of the central Pacific (CP) (Zhang, 2005).

As it propagates eastward from IO to the western Pacific (WP), MJO exerts a large-scale control on higher-frequency variability including synoptic wave trains, tropical cyclone activities and the diurnal cycle of precipitation over land (e.g., Lau and Lau, 1990; Maloney and Dickinson, 2003; Fu *et al*., 2007; Zhou and Li, 2010; Hsu *et al*., 2011). Given that MJO could exert a remote impact on global circulation (e.g., Hong and Li, 2009; Dole *et al*., 2014), it is important to understand MJO intensity change in order to improve the subseasonal (2–6 week) predictability of the Earth climate system (Waliser *et al*., 2003).

The intensity of MJO displays a strong seasonality (Madden, 1986; Wang and Rui, 1990; Zhang and Dong, 2004), an interannual variability (Salby *et al*., 1994; Slingo *et al*., 1999; Kessler, 2001; Chen *et al*., 2016; Deng and Li, 2016; Deng *et al*., 2016; Yoo and Son, 2016) and a trend (e.g., Slingo *et al*., 1999; Zveryaev, 2002; Jones and Carvalho, 2006; Tao *et al*., 2015; Wang *et al*., 2020). For example, while the MJO is dominated by eastward propagation in boreal winter, the boreal summer intraseasonal oscillation exhibits pronounced northward propagation (Jiang *et al*., 2004). The eastward propagating MJO tends to be strengthened (weakened) in the central equatorial Pacific during El Niño (La Niña) (Hendon *et al*., 1999; Kessler, 2001; Teng and Wang, 2003; Zhang, 2005). The modulation of the MJO by the interannual variability is primarily through the change of the background moisture and vertical shear (Deng *et al*., 2016; Deng and Li, 2016). Slingo *et al*. (1999) and Jones and Carvalho (2006) found that MJO appeared more active after 1976. Using century-long reanalysis datasets, Wang *et al*. (2020) noted that the boreal winter MJO intensity increases at a much greater rate than the boreal summer counterpart.

Until now, owing to limited length of the observational data, the interdecadal change of the MJO intensity with the centennial data has not been studied yet. Only Suhas and Goswami (2010) detected the multidecadal variability of MJO intensity at a roughly ~30-year periodicity with NCEP-NCAR and ERA40 reanalysis data from 1948 to 2006. The relatively short period datasets is often mixed up with the change associated with natural interdecadal modes. It is not clear whether or not the MJO intensity has a significant interdecadal change. If a significant interdecadal change does exist, what is the physical mechanism responsible for the interdecadal change. The objective of the current study is to address the questions above. The remainder of this paper is organized as follows. In section 2, two century-long reanalysis datasets and the definition of the MJO intensity are introduced. In section 3, the interdecadal variability of the MJO intensity is examined. In section 4, we further examine how the interdecadal background mean state impacts the MJO intensity. Finally, a conclusion and discussion are given in the last section.

2 | DATA AND METHOD

2.1 | Data

Two century-long reanalysis datasets were used to investigate the interdecadal variability of the MJO intensity. The first one is the Twentieth Century Reanalysis Project (hereafter 20CR; Compo *et al*., 2011) from the National Oceanic and Atmospheric Administration (NOAA). We cover a 138-year period (from 1871 to 2008). This reanalysis dataset assimilated surface observations with 56 members. Here the ensemble mean of the 56 members is used. The other one is the European Center for Medium-Range Weather Forecasts (ECMWF) atmospheric reanalysis dataset (hereafter ERA-20C; Poli *et al*., 2016). It covers a 111-year period (from 1900 to 2010). Compared to 20CR, ERA-20C provided a single member product.

Daily outgoing long-wave radiation (OLR), precipitation (precipitation rate from NOAA 20th Century, transformed to precipitation in following analysis), zonal, meridional and vertical wind, specific humidity, temperature, geopotential height and surface latent heat flux from both the reanalysis datasets were used to calculate the MJO intensity and the interdecadal background mean states. The horizontal resolution of these variables is $2^\circ \times 2^\circ$. In addition, monthly sea surface temperature (SST) field from the Hadley Center Sea Ice and Surface Temperature dataset version 1 (HadISST1; Rayner *et al*., 2003) from 1871 to 2008 with resolution of $1^\circ \times 1^\circ$ was also used.

A caution is needed in terms of the quality of the reanalysis data because of limited observations in earlier 20th century. Different from shorter-period reanalysis products such as ERA-I and NCEP II reanalysis datasets, only surface observations were assimilated into the assimilation system in 20CR and ERA-20C. Nevertheless, the MJO structure and evolution derived from the 20CR

and ERA-20C datasets appear reasonably well (Cui *et al*., 2020).

2.2 | Definition of the MJO intensity

The daily amplitude of the MJO is defined based on a Real-time MJO Multi-variate (RMM) index developed by Wheeler and Hendon (2004). It is the square root of the sum of two RMM indices squared ($\mathrm{RMM} = \sqrt{\mathrm{RMM1}^2 + \mathrm{RMM2}^2}$). The RMM indices combine the effects of the equatorial zonal winds and convection. Detailed procedures are as follows. A 20–100-day (Russell, 2006) band-pass filter was first applied to the 200 hPa, 850 hPa zonal winds and OLR anomaly fields with the climatological annual cycle and the linear trend removed. Next a multivariable EOF (empirical orthogonal function) analysis with the tropical average (15°S–15°N) was performed, to obtain two leading EOF patterns and their associated normalized principal components (RMM1 and RMM2). The calculated daily MJO intensity was then averaged over the boreal winter season (December–January–February) to represent the overall MJO intensity at a particular year. The yearly MJO intensity time series from the two reanalysis datasets were then subject to a 9-year low-pass filter to illustrate the interdecadal MJO variability (IMV). Hereafter we refer the IMV time series from 20CR and ERA-20C as IMV_20CR and IMV_ERA, respectively.

3 | INTERDECADAL VARIABILITY OF THE MJO INTENSITY

Figure 1a displays the normalized time series of the IMV indices based on the 20CR and ERA-20C datasets. Note that the two indices illustrate high similarity with the correlation coefficient .81 in detecting the active and inactive phases and amplitude of the IMV. For instance, they experienced relatively weak amplitude from 1910s to 1950s, two active phases around 1960 and 1990, and two inactive phases around 1950 and 1980, analogous to Suhas and Goswami (2010, fig. 6a). The similar temporal evolution feature revealed from the two different reanalysis products adds confidence for further investigation.

3.1 | Dominant periodicity of the IMV

A power spectrum analysis to the two time-series indices was conducted to reveal the dominant periodicity of the interdecadal MJO variation. The statistical significance of the power spectrum was tested by comparing the power spectral variance of the time series with that of the background red noise at the significance level of .05. Figure 1b shows that both the power spectra (thick curve) have a statistically significant ($p < .05$) peak at 12–20 years. The amplitude of the power spectrum obtained based on 20CR is stronger than that derived based on ERA-20C. Nevertheless, both the datasets contain the statistically significant interdecadal variability of the MJO intensity.

3.2 | Relationship with Pacific and Atlantic interdecadal modes

An interesting question is whether or not the interdecadal variability of the MJO intensity is closely related to natural interdecadal modes such as the Interdecadal Pacific Oscillation (IPO) and the Atlantic Multi-decadal Oscillation (AMO) and other well-known modes, such as El Niño–Southern Oscillation (ENSO), Pacific Decadal Oscillation (PDO) and Pacific Meridional Mode (PMM). An EOF analysis of 8-year low-pass filtered monthly global SST anomaly field was conducted to obtain three principal components. Whereas the first mode represents a clear global warming trend, the second and third modes represent the IPO and AMO, respectively. The EOF analysis was also applied to the DJF SST anomaly over North Pacific (125°E–100°W, 20°N–65°N) to get the first mode as PDO. The ENSO and PMM are, respectively, obtained

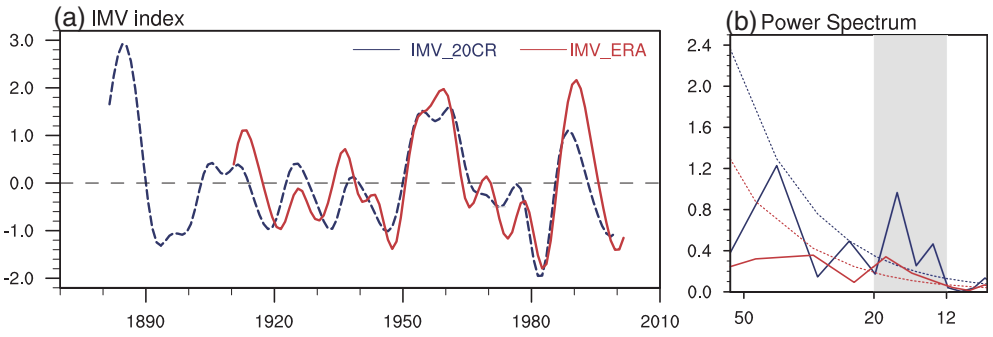

FIGURE 1 (a) Time series of the normalized 9-year low-pass filtered IMV_20CR (blue) and IMV_ERA (red) indices. (b) Power spectra of the two IMV indices (solid lines) and the 95% confidence level (dash lines). The gray shading represents significant spectrum peaks (unit: year)

from the first and second mode of singular value decomposition (SVD) with DJF SST anomaly and low-level wind vectors over the region (120°E–80°W, 32°N–21°S). The SST anomaly is defined as deviations from the monthly climatology and trend. The EOF figures are all not shown.

Table 1 lists the correlation coefficients between two IMV indices and climate modes with the reduced degrees of freedom displayed in the bracket. Whereas a weak positive (negative) correlation was found for both the reanalysis datasets, the correlation is statistically insignificant, being far less than 95% confidence level. The method used for estimating the effective sample size is based on the cross-correlation (Davis, 1976; Chen, 1982). The result suggests that the interdecadal variability of the MJO intensity is independent from the well-known climate modes, consistent with the conclusion from Suhas and Goswami (2010).

TABLE 1 Correlation coefficients between the IMV indices and other modes

	IMV_NOAA	IMV_ERA
IPO	0.19 (36)	0.13 (41)
AMO	−0.12 (46)	−0.15 (43)
PDO	0.12 (52)	0.11 (37)
PMM	0.03 (44)	0.09 (47)
Niño3.4	0.02 (92)	0.05 (72)

Note: The value in bracket represents the effective sample size for significance test.

3.3 | MJO characteristics during the active and inactive phases

To illustrate the spatial distribution and propagation characteristics of the MJO during the active and inactive phases of the IMV, we conducted a composite analysis. An active (inactive) MJO year was selected based on the threshold of 0.5 (−0.5) *SD* of the normalized IMV indices.

The IMV indice is derived based on the RMM index, which denoting the eastward propagating intraseasonal components. So the Wheeler–Kiladis space–time spectra (Wheeler and Kiladis, 1999) covering the period of 20–100 days and zonal wavenumber 1–3 was used to extract eastward propagating MJO signals. Figure 2 shows the horizontal patterns of standard deviation of space–time filtered OLR anomalies during the active and inactive phases and the difference. Both the datasets show strong MJO variabilities over the Indo-Pacific warm pool region, regardless of the interdecadal phases. The result is consistent with the observations (Wang and Rui, 1990; Zhang, 2005). The difference maps (Figure 2c,f) show clearly that the MJO activity is stronger over the equatorially IO, the Maritime Continent (MC) and the equatorial WP during the active phase than during the inactive phase.

The MJO propagation feature was also examined. Figure 3 shows the lagged time-longitude sections of the space–time filtered OLR anomalies averaged over 15°S–15°N regressed onto a reference OLR time series over the equatorial IO and western MC (90°E–120°E, 15°S–5°S). There are pronounced eastward phase propagation

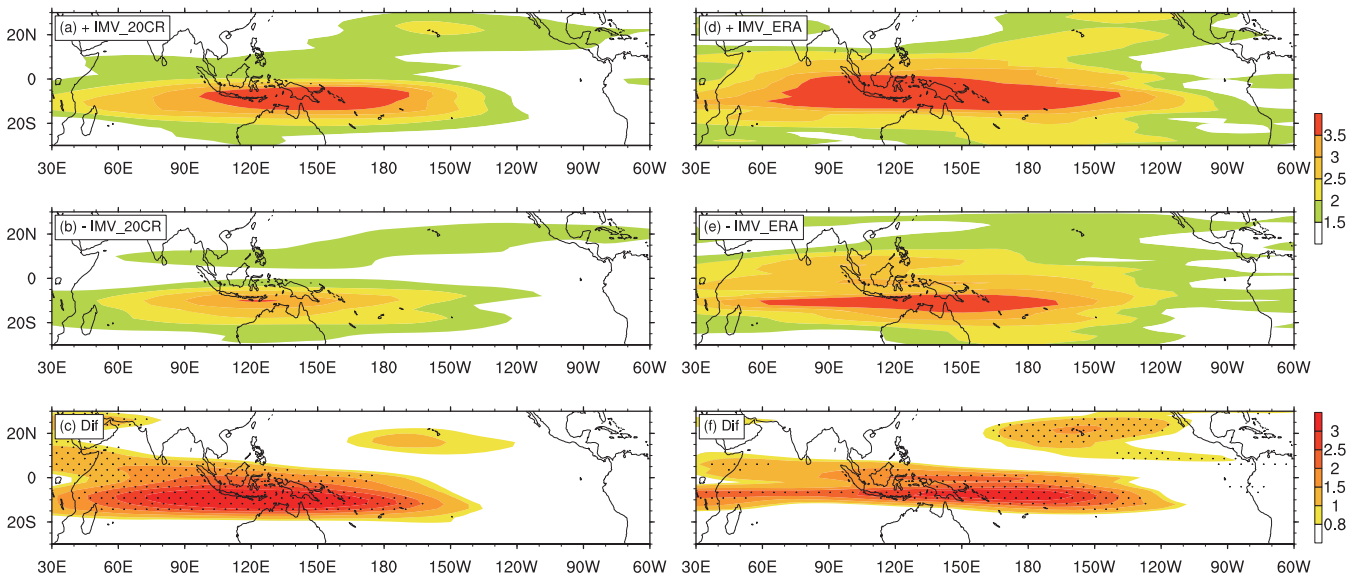

FIGURE 2 Horizontal distributions of standard deviation of space–time filtered OLR anomalies ($W \cdot m^{-2}$) during the active (top) and inactive (middle) phases derived from 20CR and ERA-20C. The bottom panels show the difference pattern (active minus inactive, areas passing 95% significance level with *t* test are dotted)

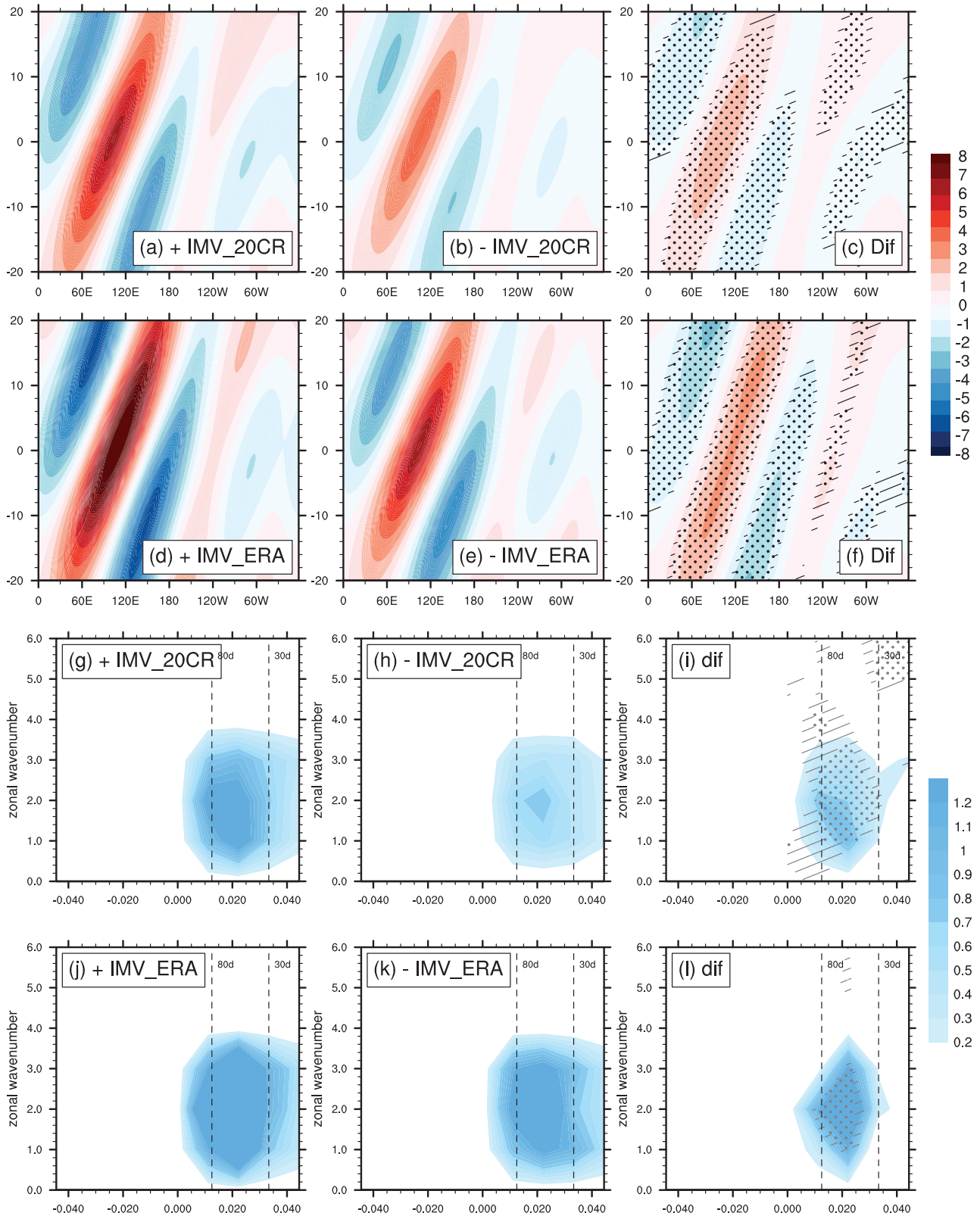

FIGURE 3 Lagged time–longitude sections (a–f) of anomalous OLR ($W \cdot m^{-2}$) field averaged over 15°S–15°N regressed onto space–time filtered OLR time series over (15°S–5°S, 90°E–120°E) and (g–l) wavenumber–frequency spectra of space–time filtered OLR during the active (a, d, g, j) and inactive (b, e, h, k) phases and (c, f, i, l) their difference (active minus inactive). The top and third panels are based on the IMV_20CR index and the second and bottom panels are based on the IMV_ERA index. The dots (hatches) denote areas exceeding 95% (90%) confidence level with *t* test

during both phases. The difference maps illustrate that the amplitude of the eastward propagating MJOs is stronger during the active phase, whereas the eastward phase speed appears similar during the two phases. The wavenumber–frequency spectra of the filtered OLR shown in Figure 3 can also support it. The power spectrum intensity differs significantly, but the frequency and wavenumber, on the other hand, have little change. This indicates that the difference of the MJO between the two interdecadal phases lies primarily in MJO intensity, not in phase propagation.

4 | CAUSE OF THE IMV

To understand the cause of the interdecadal variability of the MJO intensity, we examine the difference of the interdecadal background mean state. Due to the similar interdecadal mean state patterns from the NOAA and ERA reanalysis datasets, hereafter only the ensemble average fields with these two datasets are shown. Because of a near mirror-image mean state pattern between the active and inactive phase composite, only the differences maps between the active and inactive phases are presented hereafter.

Figure 4 shows the difference maps of the background mean precipitation, SST and 850-hPa wind fields. Enhanced precipitation centers appear over the equatorial zone (i.e., the rectangle box in Figure 4a), ranged from the equatorial IO to the WP. The enhanced mean convective region overlaps the strengthened MJO variability region shown in Figure 2c,f, implying the possible role of the interdecadal mean state change on the MJO strength.

Physically, one may argue that the strengthened precipitation may increase the background mean moisture in situ through vertical moisture advection. As the mean moisture decreases exponentially with height, ascending motion may lead to the increase of column water vapor through vertical moisture transport. The increase of the background moisture provides a more favorable condition for the development of the MJO (Hendon and Liebmann, 1994; Deng *et al*., 2016; Deng and Li, 2016).

The interdecadal change of the mean precipitation is closely associated with the change of the background mean SST and low-level wind fields. A warm SST anomaly (SSTA) appears in the equatorial CP. In response to the SSTA forcing, a large-scale low-level cyclonic wind pattern appears to the northwest of the warm SSTA, as a Rossby wave response to the anomalous heat source (Gill, 1980). At the equatorial WP there is pronounced anomalous westerly. The westerly tends to transport high mean moisture eastward, strengthening the precipitation in the WP.

It is worth mentioning that the maximum precipitation center at the equator appears slightly west of the maximum SSTA center. This is attributed to the combined effect of the mean and anomalous SST fields. While the SSTA center is located east of the dateline, the mean SST maximum is located over the WP, decaying rapidly toward the east. As a result, the total SST (i.e., the sum of the mean and anomalous SST) is largest west of the dateline. It is the total SST what determines the center of the precipitation anomaly. This scenario is in a way similar to El Niño, that is, when a maximum SSTA center associated with El Niño is located in the equatorial eastern Pacific (EP), the associated precipitation center is located in the CP (Li, 1997; Li *et al*., 2003).

Another significant warm SSTA center appears in the MC. While the amplitude of this SSTA is slightly weaker than that over the CP, its impact on local precipitation is not necessarily weak, due to the high mean SST effect.

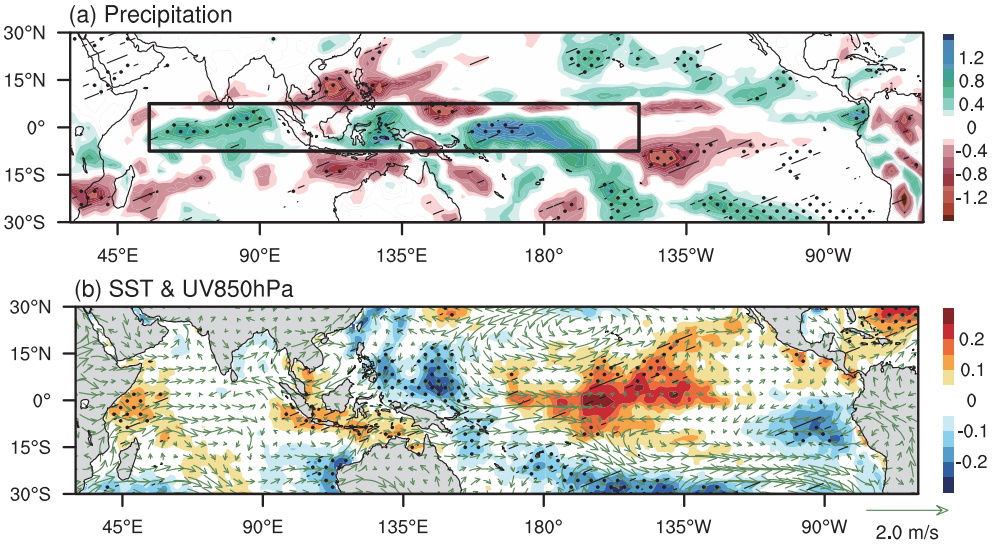

FIGURE 4 Differences of (a) the background mean precipitation (unit: mm·day^{-1}) and (b) the background mean SST (unit: K) and 850 hPa wind (gray vector; unit: m·s^{-1}) fields between the active and inactive phases of the IMV indices. The dots (hatches) denote 95% (90%) confidence level with *t* test

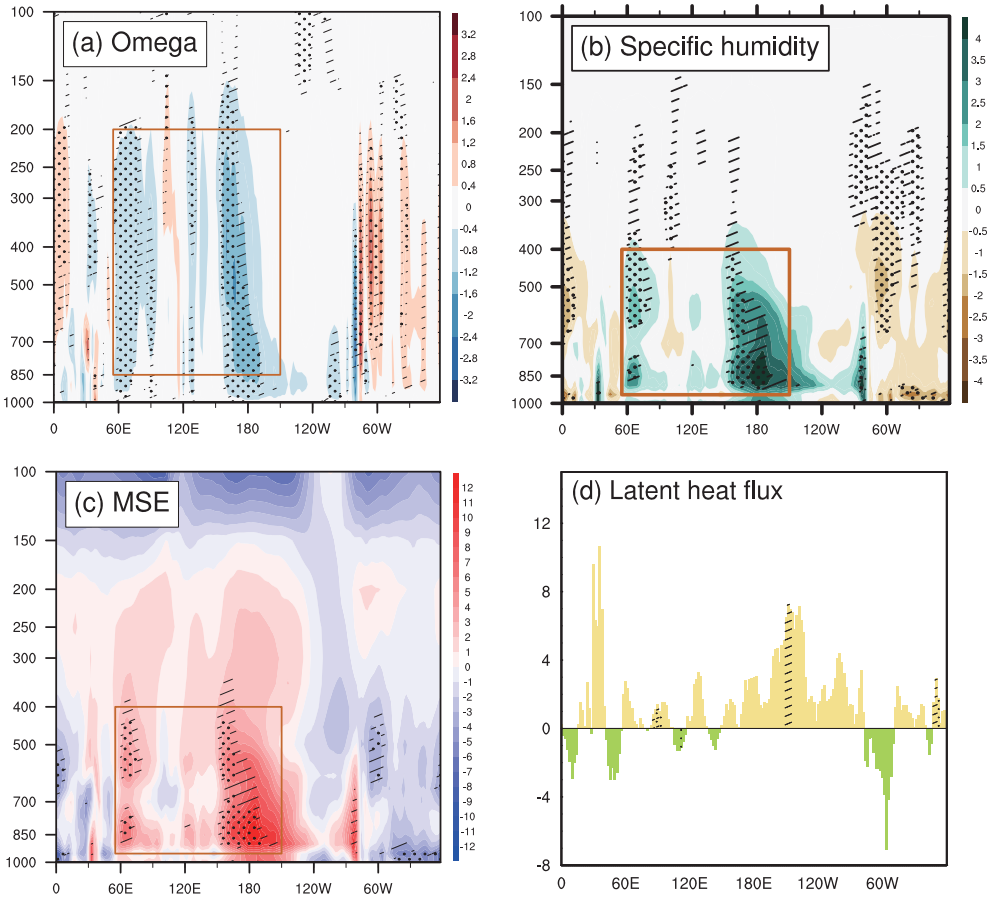

FIGURE 5 Zonal-vertical cross sections of (a) the background mean vertical *p*-velocity (omega, unit: $Pa \cdot s^{-1}$), (b) specific humidity (unit: $g \cdot kg^{-1}$) and (c) MSE (unit: $m^2 \cdot s^{-2}$) between the active and inactive phases of the IMV indices. (d) Zonal distribution of the surface latent heat flux difference (unit: $W \cdot m^{-2}$) along the equator between the active and inactive phases (active minus inactive). The dots (hatches) denote 95% (90%) confidence level with *t* test

An interesting question is what causes anomalous precipitation over the equatorial central IO, as local SSTA signal is unclear. We speculate that it is caused by local convective instability due to the increase of near surface moisture induced by enhanced surface evaporation. As we know, the mean wind over the equatorial IO is westerly. The enhanced convection over the MC causes a strengthened Walker Circulation over the IO. As a result, the low-level anomalous wind is westerly over the IO (Figure 4b). The anomalous wind, superposed on the mean westerly, leads to the increase of the surface latent heat flux in situ (Figure 5d). This leads to the increase of the near surface moisture, promoting the setup of a convectively unstable stratification and the onset of convection.

How does the strengthened background mean precipitation affect the MJO intensity? We argue that it is through the change of the background moisture and moist static energy (MSE). Figure 5a–c displays the zonal-vertical cross sections along the equator of vertical *p*-velocity (omega), specific humidity and MSE difference fields between the active and inactive phases. Here MSE is defined as $MSE = c_p T + g\varkappa + L_v q$, where T (K) is temperature, $\varkappa$ (m) is height, q (g/kg) is specific humidity, c_p is the specific heat at constant pressure (=1,004 $J \cdot K^{-1} \cdot kg^{-1}$), g is the gravitational acceleration (=9.8 $m \cdot s^{-2}$) and L_v is the latent heat of vaporization (=2.5×10^6 $J \cdot kg^{-1}$).

It is seen that strengthened ascending motion appears across the equatorial warm pool (Figure 5a), being consistent with the enhanced precipitation in situ (Figure 4a). The ascending motion favors the increase of local specific humidity (Figure 5b) through anomalous vertical moisture advection. The increase of the background moisture leads to the increase of the column MSE. As seen from Figure 5c, a positive MSE anomaly appears throughout the troposphere, with maximum amplitude near 850 hPa. If one uses the vertical difference of the MSE (or equivalent potential temperature) between lower (1,000–500 hPa) and upper troposphere (300–-100 hPa) to measure the convective instability, then one may conclude that the equatorial warm pool possesses a more unstable stratification during the active phase. Such a background environmental condition favors the development and growth of MJO-like disturbances.

To sum up, the analysis of the large-scale background mean state indicates that a warmer SST in the equatorial CP and MC during the active phase is critical in inducing enhanced precipitation, moisture and MSE over the Indo-Pacific warm pool. The change of these background

thermodynamic fields provides a favorable environmental condition for MJOs to grow. This explains why the MJO intensity experienced a marked interdecadal variability over the equatorial IO and WP.

5 | DISCUSSION AND CONCLUSION

The interdecadal variability of the MJO intensity was investigated based on two century-long reanalysis datasets (20CR and ERA-20C). The two datasets were capable of capturing the amplitude, structure and evolution characteristics of the MJO through a comparison with the observed features during the period of 1979–2008 (Wang *et al*., 2020). The DJF-mean daily RMM indices were used to represent the MJO intensity each year. The time series of the MJO intensity was subject to a 9-year low-pass filtering to represent the IMV. A power spectrum analysis of the IMV time series was conducted, and the result shows that the IMV exhibits significant peaks at 12–20-year periods. There are no significant correlations between the IMV and other climate modes.

During the active phase of the IMV, the MJO activities appear stronger across the entire equatorial warm pool expanding from the IO to the WP A lead–lag regression analysis further indicates a significant difference in the strength of the eastward propagating MJO signal between the active and inactive phases, even though there is little difference in phase propagation speed.

The distinctive interdecadal change of the MJO intensity arises from the change of the background SST, precipitation and moisture. Significant warm SST anomalies appear in the equatorial CP and the MC. This leads to enhanced precipitation over the equatorial WP and the MC. Meanwhile the enhanced Walker Circulation over the IO promotes the surface evaporation and increases near-surface moisture in situ. This promotes the setup of a convectively unstable stratification and thus the onset of convection over the equatorial IO. The enhanced background precipitation and ascending motion across the equatorial IO-WP warm pool favor the growth of MJO-like perturbations through the increase of the background moisture and MSE caused by vertical moisture/MSE advection.

While the current study emphasizes the role of the interdecadal variation of SST anomalies in causing the MJO intensity change, it is worth mentioning that a previous study by Suhas and Goswami (2010) suggested that a portion of the MJO multidecadal variability was possibly driven by internal atmospheric dynamics (through nonlinear interaction between zonal mean flow and MJO). Further in-depth theoretical and modeling studies are needed to test the aforementioned hypotheses and to understand the relative role of the atmospheric and oceanic processes in causing the observed IMV.

An open question is whether or not the favorable interdecadal mean state during the active phase arises from a combined influence of the IPO and AMO. Whereas the negative AMO phase promotes an equatorial westerly anomaly and enhanced surface evaporation over the IO, a positive IPO phase favors a positive rainfall anomaly over the WP. Another issue is given the same interdecadal background mean state, how does the intensity of the boreal summer intraseasonal oscillation change? These issues will be addressed in future endeavors.

ACKNOWLEDGEMENTS

This study was jointly supported by NSFC grant (42088101), the National Key R&D Program of China (2018YFA0605604), NSF grant (AGS-20-06553) and NOAA grant (NA18OAR4310298). This is SOEST contribution number 11230, IPRC contribution number 1500 and ESMC number 343.

ORCID

Ziyue Wang https://orcid.org/0000-0001-6624-599X

REFERENCES

Adames, Á.F., Kim, D., Sobel, A.H., Del Genio, A. and Wu, J. (2017) Changes in the structure and propagation of the MJO with increasing CO_2. *Journal of Advances in Modeling Earth Systems*, 9, 1251–1268. https://doi.org/10.1002/2017MS000913.

Chen, W.Y. (1982) Fluctuations in Northern Hemisphere 700 mb height field associated with the southern oscillation. *Monthly Weather Review*, 110, 808–823. https://doi.org/10.1175/1520-0493(1982)110<0808:finhmh>2.0.co;2.

Chen, X., Ling, J. and Li, C. (2016) Evolution of the Madden–Julian oscillation in two types of El Niño. *Journal of Climate*, 29, 1919–1934. https://doi.org/10.1175/JCLI-D-15-0486.1.

Compo, G.P., Whitaker, J.S., Sardeshmukh, P.D., Matsui, N., Allan, R.J., Yin, X., Gleason, B.E., Vose, R.S., Rutledge, G., Bessemoulin, P., Brönnimann, S., Brunet, M., Crouthamel, R.I., Grant, A.N., Groisman, P.Y., Jones, P.D., Kruk, M.C., Kruger, A.C., Marshall, G.J., Maugeri, M., Mok, H.Y., Nordli, Ø., Ross, T.F., Trigo, R.M., Wang, X.L., Woodruff, S.D. and Worley, S.J. (2011) The twentieth century reanalysis project. *Quarterly Journal of the Royal Meteorological Society*, 137 (654), 1–28. http://dx.doi.org/10.1002/qj.776.

Cui, J., Wang, L., Li, T. and Wu, B. (2020) Can reanalysis products with only surface variables assimilated capture Madden–Julian oscillation characteristics? *International Journal of Climatology*, 40, 1279–1293. https://doi.org/10.1002/joc.6270.

Davis, R.E. (1976) Predictability of sea surface temperature and sea level pressure anomalies over the North Pacific Ocean. *Journal of Physical Oceanogrphy*, 6, 249–266. https://doi.org/10.1175/1520-0485(1976)006<0249:possta>2.0.co;2.

Deng, L. and Li, T. (2016) Relative roles of background moisture and vertical shear in regulating interannual variability of boreal

summer intraseasonal oscillations. *Journal of Climate*, 29, 7009–7025. https://doi.org/10.1175/JCLI-D-15-0498.1.

Deng, L., Li, T., Liu, J. and Peng, M. (2016) Factors controlling the interannual variations of MJO intensity. *Journal of Meteorological Research*, 30, 328–340. https://doi.org/10.1007/s13351-016-5113-3.

Dole, R., Hoerling, M., Kumar, A., Eischeid, J., Perlwitz, J., Quan, X.-W., Kiladis, G., Webb, R., Murray, D., Chen, M., Wolter, K. and Zhang, T. (2014) The making of an extreme event: putting the pieces together. *Bulletin of the American Meteorological Society*, 95(3), 427–440. http://dx.doi.org/10.1175/bams-d-12-00069.1.

Fu, B., Li, T., Peng, M.S. and Weng, F. (2007) Analysis of tropical cyclone genesis in the western North Pacific for 2000 and 2001. *Weather Forecast*, 22, 763–780. https://doi.org/10.1175/WAF1013.

Gill, A.E. (1980) Some simple solutions for heat-induced tropical circulation. *Quarterly Journal of the Royal Meteorological Society*, 106, 447–462. https://doi.org/10.1002/qj.49710644905.

Hendon, H.H. and Liebmann, B. (1994) Organization of convection within the Madden–Julian oscillation. *Journal of Geophysical Research*, 99, 8073–8083. https://doi.org/10.1029/94JD00045.

Hendon, H.H., Zhang, C. and Glick, J.D. (1999) Interannual variation of the Madden–Julian oscillation during austral summer. *Journal of Climate*, 12, 2538–2550. https://doi.org/10.1175/1520-0442(1999)012<2538:ivotmj>2.0.co;2.

Hong, C.-C. and Li, T. (2009) The extreme cold anomaly over southeast Asia in February 2008: roles of ISO and ENSO. *Journal of Climate*, 22, 3786–3801.

Hsu, P.-C., Li, T. and Tsou, C.-H. (2011) Interactions between boreal summer intraseasonal oscillations and synoptic-scale disturbances over the western North Pacific. Part I: energetics diagnosis. *Journal of Climate*, 24(3), 927–941.

Jiang, X., Li, T. and Wang, B. (2004) Structures and mechanisms of the northward propagating boreal summer intraseasonal oscillation. *Journal of Climate*, 17, 1022–1039. https://doi.org/10.1175/1520-0442(2004)017<1022:SAMOTN>2.0.CO;2.

Jones, C. and Carvalho, L.M.V. (2006) Changes in the activity of the Madden–Julian oscillation during 1958–2004. *Journal of Climate*, 19, 6353–6370. https://doi.org/10.1175/JCLI3972.1.

Kessler, W.S. (2001) EOF representations of the Madden–Julian and its connection with ENSO. *Journal of Climate*, 14, 3055–3061. https://doi.org/10.1175/1520-0442(2001)014<3055:EROTMJ>2.0.CO;2.

Lau, K.-H. and Lau, N.-C. (1990) Observed structure and propagation characteristics of tropical summertime synoptic-scale disturbances. *Monthly Weather Review*, 118(9), 1888–1993.

Lau, K.-M. and Chan, P.H. (1986) Aspects of the 40–50 day oscillation during the northern summer as inferred from outgoing longwave radiation. *Monthly Weather Review*, 114, 1354–1367. https://doi.org/10.1175/1520-0493(1986)114<1354:aotdod>2.0.co;2.

Lau, K.-M. and Peng, L. (1987) Origin of low-frequency (intraseasonal) oscillations in the tropical atmosphere. Part I: basic theory. *Journal of the Atmospheric Sciences*, 44, 950–972. https://doi.org/10.1175/1520-0469(1987)044<0950:oolfoi>2.0.co;2.

Li, T. (1997) Phase transition of the El Niño–Southern Oscillation: a stationary SST mode. *Journal of the Atmospheric Sciences*, 54, 2872–2887. https://doi.org/10.1175/1520-0469(1997)054<2872:PTOTEN>2.0.CO;2.

Li, T. and Hsu, P. (2017) *Fundamentals of Tropical Climate Dynamics*. New York, NY: Springer.

Li, T. and Hu, F. (2019) A coupled moisture-dynamics model of the Madden–Julian oscillation: convection interaction with first and second baroclinic modes and planetary boundary layer. *Climate Dynamics*, 53, 5529–5546. https://doi.org/10.1007/s00382-019-04879-x.

Li, T. and Wang, B. (1994) The influence of sea surface temperature on the tropical intraseasonal oscillation: a numerical study. *Monthly Weather Review*, 122, 2349–2362. https://doi.org/10.1175/1520-0493(1994)122<2349:tiosst>2.0.co;2.

Li, T., Wang, B., Chang, C.-P. and Zhang, Y. (2003) A theory for the Indian Ocean dipole-zonal mode. *Journal of the Atmospheric Sciences*, 60, 2119–2135.

Li, T. and Zhou, C. (2009) Planetary scale selection of the Madden–Julian oscillation. *Journal of the Atmospheric Sciences*, 66, 2429–2443. https://doi.org/10.1175/2009JAS2968.1.

Madden, R.A. (1986) Seasonal variations of the 40–50 day oscillation in the Tropics. *Journal of the Atmospheric Sciences*, 43, 3138–3158. https://doi.org/10.1175/1520-0469(1986)043<3138:SVOTDO>2.0.CO;2.

Madden, R.A. and Julian, P.R. (1971) Detection of a 40–50 day oscillation in the zonal wind in the tropical Pacific. *Journal of the Atmospheric Sciences*, 28, 702–708. https://doi.org/10.1175/1520-0469(1971)028<0702:doadoi>2.0.co;2.

Madden, R.A. and Julian, P.R. (1972) Description of global-scale circulation cells in the tropics with a 40–50 day period. *Journal of the Atmospheric Sciences*, 29, 1109–1123. https://doi.org/10.1175/1520–0469(1972)029<1109:dogscc>2.0.co;2.

Maloney, E.D. and Dickinson, M.J. (2003) The intraseasonal oscillation and the energetics of summertime tropical western North Pacific synoptic-scale disturbances. *Journal of the Atmospheric Sciences*, 60(17), 2153–2168.

Poli, P., Hersbach, H., Dee, D.P., Berrisford, P., Simmons, A.J., Vitart, F., Laloyaux, P., Tan, D.G.H., Peubey, C., Thépaut, J.-N., Trémolet, Y., Hólm, E.V., Bonavita, M., Isaksen, L. and Fisher, M. (2016) ERA-20C: an atmospheric reanalysis of the twentieth century. *Journal of Climate*, 29(11), 4083–4097. http://dx.doi.org/10.1175/jcli-d-15-0556.1.

Rayner, N.A., Parker, D.E., Horton, E.B., Folland, C.K., Alexander, L.V., Rowell, D.P., Kent, E.C. and Kaplan, A. (2003) Global analyses of sea surface temperature, sea ice, and night marine air temperature since the late nineteenth century. *Journal of Geophysical Research: Atmospheres*, 108, 4407. https://doi.org/10.1029/2002jd002670.

Russell, D.R. (2006) Development of a time-domain, variable-period surface-wave magnitude measurement procedure for application at regional and teleseismic distances, part I: theory. *Bulletin of the Seismological Society of America*, 96, 665–677. https://doi.org/10.1785/0120050055.

Salby, M.L., Garcia, R.R. and Hendon, H.H. (1994) Planetary-scale circulations in the presence of climatological and wave-induced heating. *Journal of the Atmospheric Sciences*, 51, 2344–2367. https://doi.org/10.1175/1520-0469(1994)051<2344:pscitp>2.0.co;2.

Slingo, J.M., Rowell, D.P., Sperber, K.R. and Nortley, F. (1999) On the predictability of the interannual behaviour of the Madden–Julian oscillation and its relationship with El Niño. *Quarterly Journal of the Royal Meteorological Society*, 125, 583–609. https://doi.org/10.1256/smsqj.55410.

Sperber, K.R. (2003) Propagation and the vertical structure of the Madden–Julian oscillation. *Monthly Weather Review*, 131, 3018–3037. https://doi.org/10.1175/1520-0493(2003)131<3018:PATVSO>2.0.CO;2.

Suhas, E. and Goswami, B.N. (2010) Loss of significance and multidecadal variability of the Maddem–Julian oscillation. *Journal of Climate*, 23(13), 3739–3751.

Tao, L., Zhao, J. and Li, T. (2015) Trend analysis of tropical intraseasonal oscillations in the summer and winter during 1982–2009. *International Journal of Climatology*, 35, 3969–3978. https://doi.org/10.1002/joc.4258.

Teng, H. and Wang, B. (2003) Interannual variations of the boreal summer intraseasonal oscillation in the Asian-Pacific region. *Journal of Climate*, 16, 3572–3584. https://doi.org/10.1175/1520-0442(2003)016<3572:IVOTBS>2.0.CO;2.

Waliser, D.E., Lau, K.M., Stern, W. and Jones, C. (2003) Potential predictability of the Madden–Julian oscillation. *Bulletin of the American Meteorological Society*, 84, 33–50. https://doi.org/10.1175/BAMS-84-1-33.

Wang, B. and Li, T. (1994) Convective interaction with boundary-layer dynamics in the development of a tropical intraseasonal system. *Journal of the Atmospheric Sciences*, 51, 1386–1400. https://doi.org/10.1175/1520-0469(1994)051<1386:ciwbld>2.0.co;2.

Wang, B. and Rui, H. (1990) Dynamics of the coupled moist Kelvin–Rossby wave on an equatorial β-plane. *Journal of the Atmospheric Sciences*, 47, 397–413. https://doi.org/10.1175/1520–0469(1990)047<0397:dotcmk>2.0.co;2.

Wang, L., Li, T., Maloney, E. and Wang, B. (2017) Fundamental causes of propagating and nonpropagating MJOs in MJOTF/GASS models. *Journal of Climate*, 30, 3743–3769. https://doi.org/10.1175/JCLI-D-16-0765.1.

Wang, Z., Li, T., Gao, J. and Peng, M. (2020) Enhanced winter and summer trend difference of Madden–Julian oscillation intensity since 1871. *International Journal of Climatology*, 40, 6369–6381. https://doi.org/10.1002/joc.6586.

Wheeler, M. and Kiladis, G.N. (1999) Convectively coupled equatorial waves: analysis of clouds and temperature in the wavenumber–frequency domain. *Journal of the Atmospheric Sciences*, 56, 374–399. https://doi.org/10.1175/15200469(1999)056%3c0374:CCEWAO%3e2.0.CO;2.

Wheeler, M.C. and Hendon, H.H. (2004) An all-season real-time multivariate MJO index: development of an index for monitoring and prediction. *Monthly Weather Review*, 132, 1917–1932. https://doi.org/10.1175/1520-0493(2004)132<1917:AARMMI>2.0.CO;2.

Yoo, C. and Son, S.W. (2016) Modulation of the boreal wintertime Madden–Julian oscillation by the stratospheric quasi-biennial oscillation. *Geophysical Research Letters*, 43, 1392–1398. https://doi.org/10.1002/2016GL067762.

Zhang, C. (2005) Madden–Julian oscillation. *Reviews of Geophysics*, 43, 1–36. https://doi.org/10.1029/2004RG000158.

Zhang, C. and Dong, M. (2004) Seasonality in the Madden–Julian oscillation. *Journal of Climate*, 17, 3169–3180. https://doi.org/10.1175/1520-0442(2004)017<3169:SITMO>2.0.CO;2.

Zhao, C., Li, T. and Zhou, T. (2013) Precursor signals and processes associated with MJO initiation over the tropical Indian Ocean. *Journal of Climate*, 26, 291–307. https://doi.org/10.1175/JCLI-D-12-00113.1.

Zhou, C. and Li, T. (2010) Upscale feedback of tropical synoptic variability to intraseasonal oscillations through the nonlinear rectification of the surface latent heat flux. *Journal of Climate*, 23, 5738–5754. https://doi.org/10.1175/2010JCLI3468.1.

Zveryaev, I.I. (2002) Interdecadal changes in the zonal wind and the intensity of intraseasonal oscillations during boreal summer Asian monsoon. *Tellus A: Dynamic Meteorology and Oceanography*, 54, 288–298. https://doi.org/10.1034/j.1600-0870.2002.00235.x.

How to cite this article: Wang Z, Li T, Sun Y. Interdecadal variability of intensity of the Madden–Julian oscillation. *Atmos Sci Lett*. 2021;22: e1027. https://doi.org/10.1002/asl.1027